NANO LETTERS

2006
Vol. 6, No. 8
1699−1705

Real-Time Observation of Tubule Formation from Amorphous Carbon Nanowires under High-Bias Joule Heating

J. Y. Huang,*,† S. Chen,† Z. F. Ren,† G. Chen,‡ and M. S. Dresselhaus§

Department of Physics, Boston College, Chestnut Hill, Massachusetts 02467, and Department of Mechanical Engineering, Department of Physics, and Department of Electrical Engineering and Computer Science, Massachusetts Institute of Technology, Cambridge, Massachusetts 02139

Received May 2, 2006; Revised Manuscript Received June 20, 2006

ABSTRACT

The tubule formation process from amorphous carbon nanowires under high-bias-caused Joule heating was observed in real time in a high-resolution transmission electron microscope. The crystallization of the amorphous carbon nanowires occurred in two distinct ways: the formation of tubular graphitic basal planes parallel to the nanowire axis on the surface and the formation of nano-onions in the interior of the nanowire. The tubule formation mechanism is a process of solid-state atom diffusion at high temperatures. Energetically, the tubule formation is caused by the exceptionally low surface energy of the (0002) plane of graphite. Higher input power to the amorphous nanowires generally leads to improved graphitization and, in turn, to increased conductance. The results suggest that nanotube formation in the arc-discharge growth process may involve the formation and crystallization of amorphous carbon.

I. Introduction. Carbon nanotubes are promising candidates for use in nanoelectronics, sensors, and nanocomposites.[1−13] Despite their important applications, the nanotube growth mechanisms, particularly the noncatalytic growth by arc-discharge, remains unknown. Among the several proposed growth mechanisms, one is the open-ended growth model,[14] which assumes that pentagon and hexagon rings were formed first, followed by carbon atom additions to the reactive dangling bonds at the edge of the open-ended nanotubes. A two-step growth mechanism based on the complex structures observed by high-resolution transmission electron microscopy (HRTEM) was proposed.[15] According to this model, different amorphous carbon (a−C) nanostructures were formed first, which then crystallized into nanotubes or other tubular structures. More recently, it was suggested that nanotubes are crystallized from liquid carbon based on the observation of a viscous liquid like a−C beads present on the nanotube surface.[16] All of the previous observations were conducted on the post-grown samples, and real-time observation of the noncatalytic tubule formation process was not achieved previously.

In this paper, the real-time observation of the tubule formation processes from a−C nanowires under high-bias-caused Joule heating is reported for the first time. Individual a−C nanowires were grown in situ by electron-beam deposition inside a HRTEM. The a−C nanowires were then resistively heated to high temperatures by applying a high-bias voltage. Upon heating, the a−C nanowires crystallized into tubular structures similar to multiwall carbon nanotubes (MWCNTs) synthesized by arc-discharge. The results may suggest that nanotubes produced by arc-discharge involve the crystallization of a−C, which agrees with the two-step growth model.[15]

II. Experiments. Our experiments were conducted inside a JEOL 2010F HRTEM equipped with a Nanofactory TEM-STM system, which integrates a fully functional scanning tunneling microscope (STM) into a HRTEM. The STM probe is controlled by a piezo manipulator that can approach individual nanotubes or nanowires inside the HRTEM.[17−19] Here we grew individual a−C nanowires on the STM tip by electron-beam deposition. As the electron beam was focused to about 10 nm on the STM tip and then moved slowly forward, an a−C nanowire formed behind. The carbon source comes from either the decomposition of the hydrocarbon in the HRTEM column or from the organic impurities adsorbed on the STM probe or from both. After growth, the nanowire was bonded to another electrode by deposition of a−C between the nanowire tip and the electrode and then

* Corresponding author. E-mail: huangje@bc.edu.
† Boston College.
‡ Department of Mechanical Engineering, Massachusetts Institute of Technology.
§ Department of Physics and Department of Electrical Engineering and Computer Science, Massachusetts Institute of Technology.

10.1021/nl0609910 CCC: $33.50
Published on Web 07/20/2006

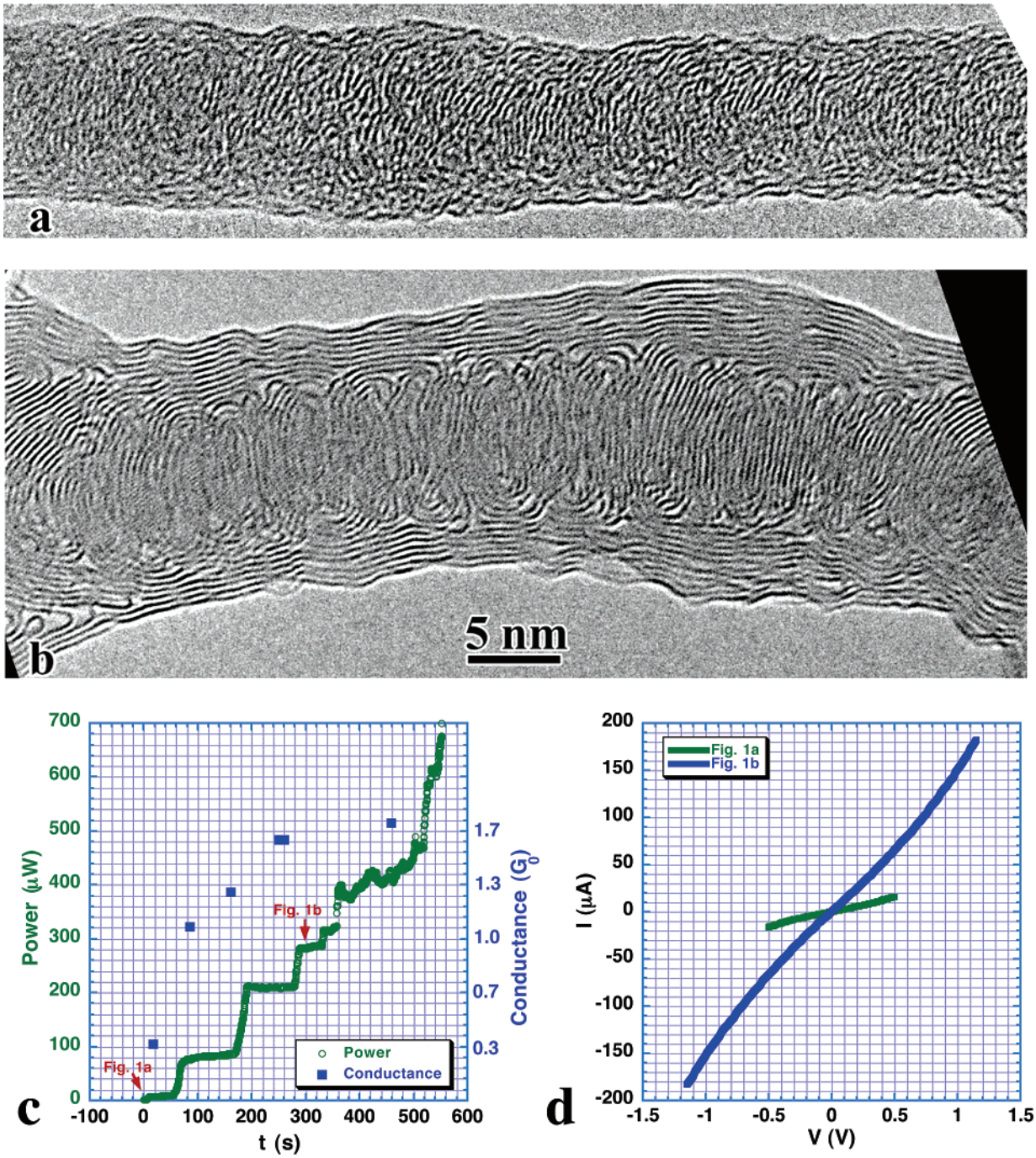

Figure 1. Crystallization of an a−C nanowire into a tubular structure. (a) The initial nanowire produced by electron-beam deposition. The length of the nanowire is about 90 nm. (b) Crystallized tubular structure at a power of 280 μW. (c) Input power, conductance vs time plot. Labels "Figure 1a" and "Figure 1b" in the curve mark when the images shown in (a) and (b) were taken. (d) $I-V$ curves labeled with "Figure 1a" and "Figure 1b" correspond to the nanowire (a) and the tubular structure (b), respectively. The low-bias conductance is $0.3G_0$ and $1.6G_0$ for the nanowire (a) and the tubular structure (b), respectively.

resistively heated to temperatures higher than 2000 °C by applying a high-bias voltage.[17−19]

III. Results and Discussion. Figure 1a shows an a−C nanowire with a diameter of about 10 nm and a length of about 90 nm. With increasing power (Figure 1c), crystallization of the a−C took place in two distinct manners: the a−C on the outside surface of the nanowire crystallized into a tubular structure with the curved graphitic basal planes parallel to the nanowire axis, while the a−C in the interior of the nanowire crystallized into nano-onions (Figure 1b), which is closely related to the preexisting short-range ordering (graphitic layers up to about 3 nm parallel to the axis on the surface but perpendicular to axis in the interior) in the originally formed a−C nanowire (Figure 1a).

With increasing power, the graphene layers in both the tubular structure and the nano-onions become more continuous and parallel. The tubular structures eventually broke from the left contact (not shown) at a power of 700 μW. Interestingly, wall-by-wall burning[19−22] was not observed in these tubular structures, possibly because they are too

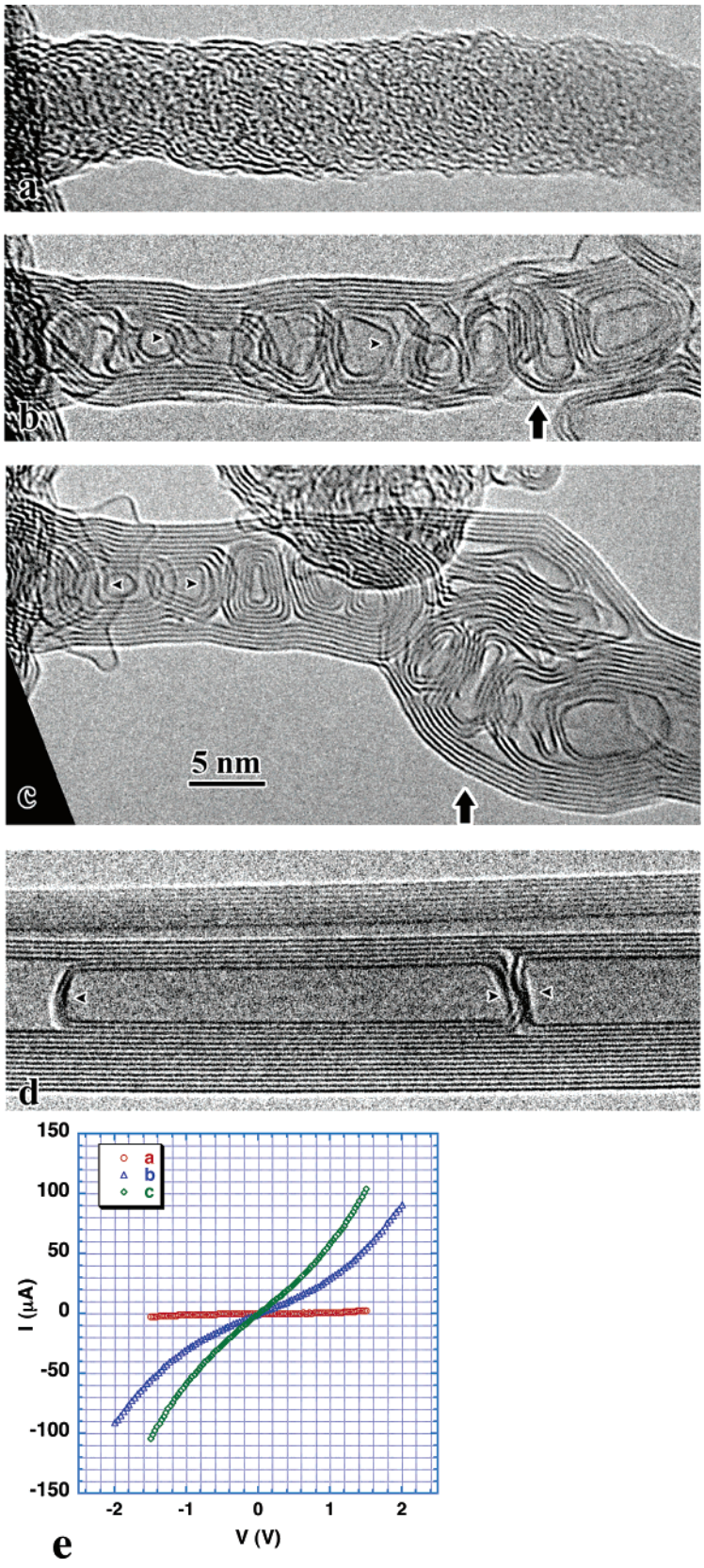

Figure 2. Crystallization of an a−C nanowire into a tubular structure. (a) An a−C nanowire with a diameter of about 8 nm and a length of 200 nm produced by electron-beam deposition. (b) After crystallization of a at 180 μW. The arrow points out a breakdown point. (c) The broken tube in (b) was reconnected (pointed out by an arrow) and crystallized at 320 μW. Note that the complicated internal tubular structures [pointed out by arrowheads in (b) and (c)] are similar to those usually observed in arc-discharged MWCNTs [pointed out by arrowheads in (d)]. (e) $I-V$ curves labeled with "a", "b", and "c" correspond to the nanostructures shown in (a), (b), and (c), respectively. The low-bias conductance of the nanostructures shown in (a)−(c) is $0.01G_0$, $0.3G_0$, and $0.6G_0$, respectively.

defective, and they usually broke in a catastrophic manner once a high-bias voltage was applied.

With increasing power and improving graphitization, the low-bias conductance of the nanostructures increases continuously until it saturates at $1.7G_0$ (Figure 1c), where G_0 is the quantum conductance. The steady-state increase of the electric conductivity is attributed to the improvement of both the contact and the graphitization of the tube caused by the increased Joule heating at increased input power. Whether the contact or the graphitization of the tube dominates the increased conductance is difficult to clarify because of the two-terminal measurement arrangement. But the contact resistance in our system is generally less than 10 kΩ. The current−voltage ($I-V$) curves are always linear at low-bias voltages (Figure 1d), indicating that an Ohmic contact was established. The $I-V$ curves turn slightly nonlinear at high-bias voltages, which may be attributed to the electron phonon scattering at increased bias voltages.[23]

Figure 2 shows the crystallization of another a−C nanowire into a tubular structure on its surface and nano-onions in the interiors at 180 μW (Figure 2b). The nanowire broke near the right of Figure 2b (see an arrow) because of electric breakdown. We then reconnected the two broken segments by depositing a−C at the broken point. The nanowire crystallized at 320 μW into a well-graphitized tubular structure containing nano-onions in contact with one another in the core of the tube (Figure 2c). Again, the formation of a tube on the surface, but onions in the interior, is related to the preexisting short-range ordering (Figure 2a).

We found that the low-bias conductance is increased from $0.01G_0$ (Figure 2a) to $0.3G_0$ (Figure 2b), and to $0.6G_0$ (Figure 2c) with increasing power. The extremely low conductance in the original a−C nanowire (Figure 2a) is rare and is very possibly caused by a high contact resistance. In this case, we were unable to deposit a−C between the nanowire and the left electrode, which might cause the high contact resistance. The $I-V$ curves are again linear at low-bias voltages and slightly nonlinear at high-bias voltages (Figure 2e).

The tubular structures (Figures 1b, 2b, and 2c) are somewhat similar to that of a MWCNT produced by arc-discharge as shown in Figure 2d. However, the quality of the tubular structure obtained by Joule heating (Figures 1b and 2c) is not as good as the nanotube produced by arc-discharge. This is likely caused by the lower temperatures associated with the Joule heating used here when compared to arc-discharge, which are estimated to be between 2000 and 3000 °C in the former[17−19] and above 4000 °C in the latter.[2] The most significant observation is that the crystallization of a−C nanowires occurred in two distinct ways; namely, the surface regions crystallized into a tubular structure similar to that of a MWCNT, while the interior crystallized into nano-onions, which is closely related to the preexisting short-range ordering of carbon atoms in the a−C nanowire. The crystallization of an a−C nanowire into tubular structures can explain many of the complicated structural features observed in the arc-discharged MWCNTs, such as the internal smaller tubes (Figure 2d) or onions inside the main tubes.

Crystallization of a−C can also lead to epitaxial growth of MWCNTs. Figure 3 shows thickening of a MWCNT through repeated crystallization of a−C. The initial MWCNT (Figure 3a) is coated with a thin layer of a−C due to electron-beam deposition. At 377 μW, two additional walls were grown epitaxially along the surface of the original MWCNT (Figure 3b). We then deposited a−C on the surface of the newly formed MWCNT again (Figure 3c), and six more walls were grown at 480 μW (Figure 3d). The $I-V$ curves from the initial a−C-coated MWCNTs (Figure 3a and c) were not recorded, but those from the well-graphitized MWCNTs were recorded (Figure 3e), and they exhibit a similar profile. The conductance is increased only slightly from $0.5G_0$ (Figure 3b) to $0.6G_0$ (Figure 3d), even though the number of walls increased from 9 (Figure 3b) to 14 walls (Figure 3d). This may be attributed to the fact that many of the inner walls were not participating in conduction because of the encapsulation of the tip of the nanotube (not shown).

The graphitization process can occur in a very short time. Figure 4 shows the graphitization of a highly disordered MWCNT. A disordered nanotube (Figure 4a) crystallized into a highly graphitized nanotube (Figure 4b) quickly within 50 milliseconds when an $I-V$ measurement was conducted (Figure 4e). Interestingly, a kink and overshooting of the nanotube walls were observed, these being characteristic structural features that are frequently observed in arc-discharged MWCNTs. After annealing at 350 μW for 3 min, the nanotube walls became straighter and the kink almost disappeared (Figure 4c). This indicates that the kink is a nonequilibrium structure. The internal overshooting walls are well developed and can be seen more clearly after annealing. For comparison, an overshooting of layers in an arc-discharged MWCNT is also presented (Figure 4d). The similarity between the two tubes (Figure 4c and d) is clear.

The tubule formation is an entirely diffusion process, different from the liquid or vapor carbon tube formation models.[14,16] The noncatalytic graphitization observed here can occur only at temperatures above 2500 °C in the heat treatment of a−C.[24] Intensive electron-beam radiation can also induce graphitization of a−C.[25,26] But electron-beam radiation of an a−C nanowire without applying a bias voltage never produced a tubular structure; instead, it produced discontinuous graphene ripples with lengths less than a few nanometers, such as those shown in Figures 1a and 2a. In fact, room-temperature radiation of perfect nanotubes always leads to the rupture of the perfect cylindrical graphene layers.[26] Therefore, we conclude that it is the high temperatures induced by high-bias voltages, not the electron-beam radiation, that produced the tubular structure. At high temperatures, diffusion is very active, leading to the crystallization of the nanowires. The present results prove clearly that for this case the whole nanotube develops simultaneously rather than initiating at one end and then growing toward the other end. The replication of the characteristic features that are frequently observed in arc-discharged MWCNTs, such as kinks (Figure 4b), smaller tubes (Figure 3d), or nano-

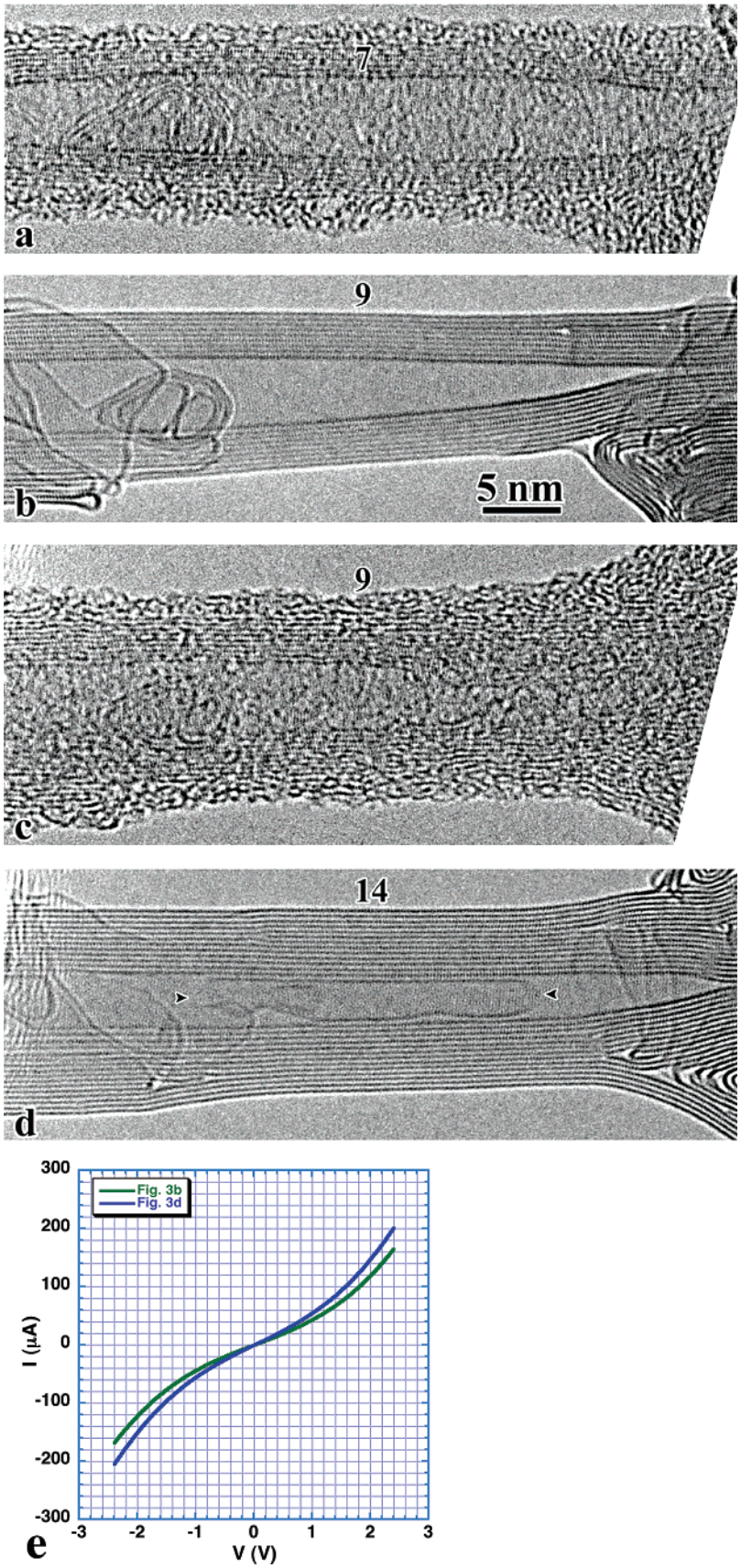

Figure 3. Epitaxial growth of nanotube walls from a−C. (The numbers indicate the total number of walls.) The length of the nanotube is 57 nm. (a) A MWCNT with 7 walls covered by a−C on its surface. (b) After epitaxial crystallization of (a) at 377 μW. (c) A second coating of a−C by electron-beam deposition on the nanotube in (b). (d) After crystallization of (c) at 480 μW. The nanotube now has 14 walls. (e) $I-V$ curves for the nanotubes shown in (b) and (d), respectively. Note that a single wall nanotube (pointed out by arrowheads) is present in the interior of the main tube. The conductance for the nanotube shown in (b) and (d) is $0.5G_0$ and $0.6G_0$, respectively.

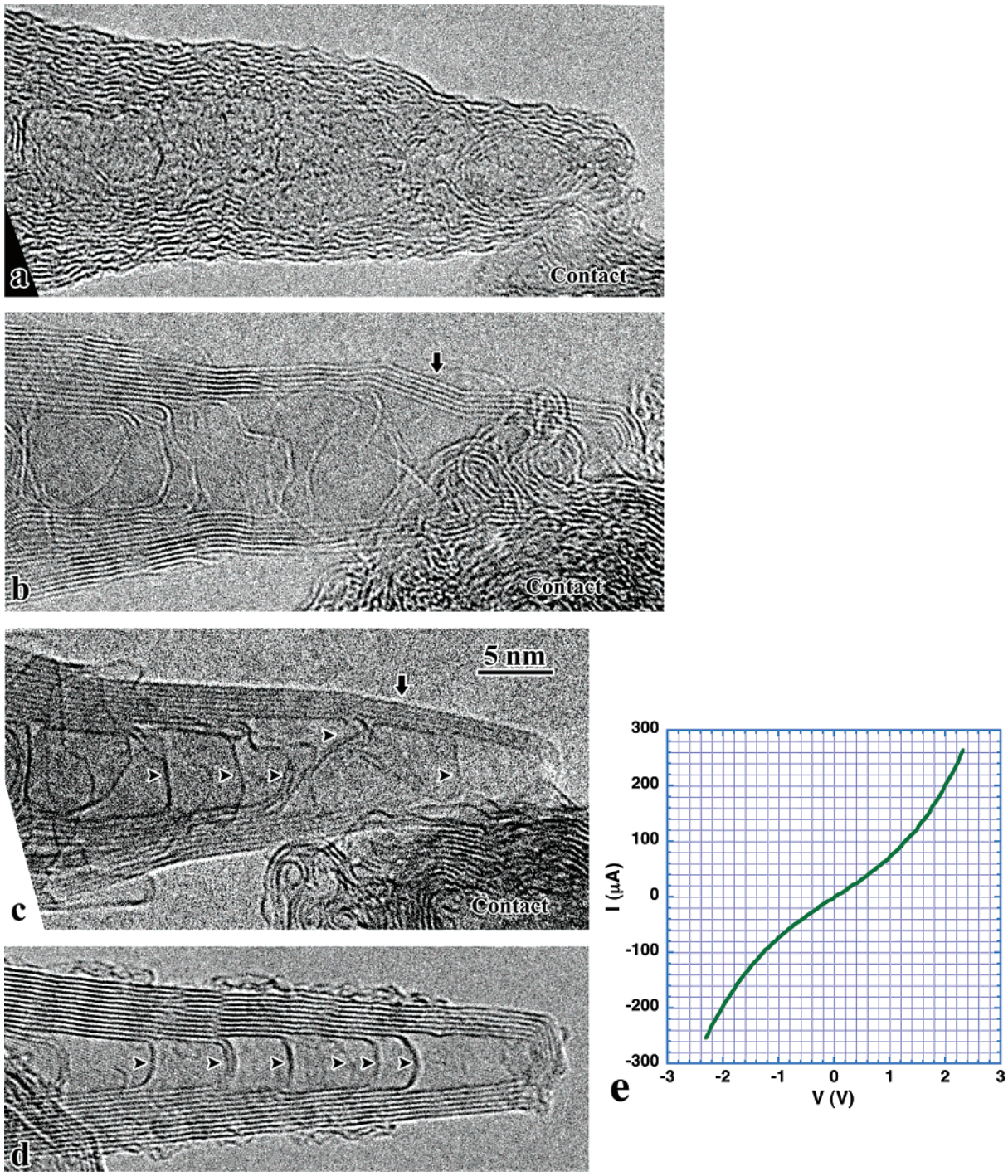

Figure 4. Crystallization of a disordered nanotube caused by an $I-V$ measurement. (a) A nanotube with disordered wall structures. (b) Crystallization of (a) caused by making an $I-V$ measurement as shown in (e). The arrowhead indicates a kink formed during the crystallization process. (c) The graphitization of (b) was improved after holding at a high power (350 μW) for 3 min. Note overshooting of layers (pointed out by arrowheads) in the interior of the nanotube, a structural feature that was frequently observed in arc-discharged nanotubes as pointed out by arrowheads in (d). (e) The $I-V$ curve that caused the crystallization of (a).

onions inside the main tubes (Figures 1b and 2c), and overshooting of layers (Figure 4c), clearly indicate the similarity between the Joule heating and the arc-discharge procedures; namely, they both involve high current, high electric field, and high temperatures. It is noted that the electric field in arc-discharge ($\sim$0.01 V/μm)[2] is generally two to four orders lower than that in the high-bias Joule heating (1$-$100 V/μm). Nevertheless, the Joule-heating-induced tubule formation may provide some insight into the growth mechanisms of arc-discharged nanotubes.

The tubule formation can be explained in terms of surface energy.[27] The (0002) plane of graphite has an exceptionally low surface energy of $\sim$77 erg/cm^2, whereas typical prismatic planes perpendicular to (0002) have a surface energy of over 4000 erg/cm^2.[27] Therefore, the tubular structure has the lowest energy when its surface is the graphite basal planes.

The formation of a tubular structure on the nanowire surface and nano-onions in the nanowire core may be attributed to the following two reasons. First, preferred orientation of graphitic layers, that is, either parallel (on the surface) or perpendicular (in the core) to the nanowire axis, exists initially in the a−C nanowire. This naturally leads to the growth of the graphitic layers along two different directions at high temperatures. Second, the crystallization of the nanowire core is confined within the tubular structure, and it is influenced by the compression stress imparted by the outer tubular structure. Indeed, it was reported recently that the pressure build-up in the nanotube hollow could be as high as 40 GPa when nanotubes are radiated at high temperatures.[28] Therefore, it is expected that the inner core can crystallize into a structure with a high-energy configuration. We believe that electromigration is not playing a role in the graphitization process because no structure difference was observed when the polarity of the bias voltage was reversed.

Acknowledgment. The work is sponsored by DOE DE-FG02-00ER45805 (Z.F.R.), DE-FG02-02ER45977 (G.C.), NSF NIRT 0304506 (Z.F.R.), NIRT 0506830 (G.C., J.Y.H., Z.F.R., and M.S.D.), and DMR-04-05538 (M.S.D.). J.Y.H. thanks Professor M. Vaziri at University of Michigan-Flint for providing the arc-discharged MWCNTs.

References

(1) Iijima, S. *Nature* **1991**, *354*, 56.
(2) Ebbesen, T. W. *Carbon Nanotubes: Preparation and Properties*; CRC Press: New York, 1997.
(3) Dresselhaus, M. S.; Dresselhaus, G.; Avouris, P. *Carbon Nanotubes: Synthesis, Structure, Properties, and Applications*; Springer: Heidelberg, 2001.
(4) Treacy, M. J.; Ebbesen, T. W.; Gibson, J. M. *Nature* **1996**, *381*, 678.
(5) Poncharal, P.; Wang, Z. L.; Ugarte, D.; de Heer, W. A. *Science* **1999**, *283*, 1513.
(6) Wong, E. W.; Sheehan, P. E.; Lieber, C. M. *Science* **1997**, *277*, 1971.
(7) Yakobson, B. I.; Smalley, R. E. *Am. Sci*. **1997**, *85*, 324.
(8) Berber, S.; Kwon, Y. K.; Tomanek, D. *Phys. Rev. Lett.* **2000**, *84*, 4613.
(9) Chiu, H. Y.; Deshpande, V. V.; Postma, H. W. C.; Lau, C. N.; Miko, C.; Forro, L.; Bockrath, M. *Phys. Rev. Lett*. **2005**, *95*, 226101.
(10) Dekker, C. *Phys. Today* **1999**, *52*, 22.
(11) Rinzler, G.; Hafner, J. H.; Nikolaev, P.; Lou, L.; Kim, S. G.; Tomanek, D.; Nordlander, P.; Colbert, D. T.; Smalley, R. E. *Science* **1995**, *269*, 1550.
(12) de Heer, W. A.; Châtelain, A.; Ugarte, D. *Science* **1995**, *270*, 1179.
(13) Baughman, R. H.; Zakhidov, A. A.; de Heer, W. A. *Science* **2002**, *297*, 787.
(14) Iijima, S.; Ajayan, P. M.; Ichihashi, T. *Phys. Rev. Lett*. **1992**, *69*, 3100.
(15) Zhou, D.; Chow, L. *J. Appl. Phys*. **2003**, *93*, 9972.
(16) de Heer, W. A.; Poncharal, P.; Berger, C.; Gezo, J.; Song, Z. M.; Bettini, J.; Ugarte, D. *Science* **2005**, *307*, 907.
(17) Huang, J. Y.; Chen, S.; Wang, Z. Q.; Kempa, K.; Wang, Y. M.; Jo, S. H.; Chen, G.; Dresselhaus, M. S.; Ren, Z. F. *Nature* **2006**, *439*, 281.
(18) Chen, S.; Huang, J. Y.; Wang, Z.; Kempa, K.; Chen, G.; Ren, Z. F. *Appl. Phys. Lett.* **2005**, *87*, 263107.
(19) Huang, J. Y.; Chen, S.; Jo, S. H.; Wang, Z.; Han, D. X.; Chen, G.; Dresselhaus, M. S.; Ren, Z. F. *Phys. Rev. Lett*. **2005**, *94*, 236802.
(20) Poncharal, P.; Berger, C.; Yi, Y.; Wang, Z. L.; de Heer, W. A. *J. Phys. Chem. B* **2002**, *106*, 12104.
(21) Collins, P. G.; Hersam, H.; Arnold, M.; Martel, R.; Avouris, P. *Phys. Rev. Lett.* **2001**, *86*, 3128.
(22) Bourlon, B.; Glattli, D. C.; Placais, B.; Berroir, J. M.; Miko, C.; Forro, L.; Bachtold, A. *Phys. Rev. Lett.* **2004**, *92*, 26804.
(23) Yao, Z.; Kane, C. L.; Dekker, C. *Phys. Rev. Lett*. **2004**, *84*, 2941.
(24) Kelly, B. T. *Physics of Graphite*; Applied Science Publisher: London, 1981.
(25) Banhart, F. *Nano. Lett.* **2001**, *1*, 329.
(26) Banhart, F. *Rep. Prog. Phys*. **1999**, *62*, 1181.
(27) Tibbetts, G. G. *J. Cryst. Growth* **1984**, *66*, 632.
(28) Sun, L.; Banhart, F.; Krasheninnikov, A. V.; Rodriguez-Manzo, J. A.; Terrones, M.; Ajayan, P. M. *Science* **2006**, *312*, 1199.

NL0609910